Project TMA4195 - Mathematical Modelling, fall 2022

Abstract

In this project we model a signal transmission in a synapse, and implement numerical schemes for computation of the concentration of neurotransmitters as a function of time and space. The time it takes for a signal to be transmitted is estimated numerically, and compared to a characteristic time scale of the processes involved. A geometrical model of the synaptic cleft is proposed, and the system is simulated for models of varying complexity.
The code for this project found in this repository.

1. Introduction

A synapse is where an axon terminal from one neuron and a dendrite spine from another neuron are close enough to communicate. The axon terminal releases neurotransmitters that the receptor molecules on the surface of the dendrite spine connect with. The neurotransmitters in the axon terminal are contained in synaptic vesicles. Each vesicle has a relatively constant number of transmitters [1]. All neurotransmitters in a vesicle are released at once.

When the transmitters are released, they diffuse freely over the synaptic cleft. The synaptic cleft is the area between the presynaptic and the postsynaptic neuron. When sufficiently many receptors on the surface of the post-terminal membrane are bounded with a transmitter, a new signal forms in the postsynaptic neuron and propagates through the axon. When a signal is transmitted, the synaptic cleft must be emptied for neurotransmitters before a new signal can form. This is done by the glia cells. The glia cells absorbs the remaining transmitters and return them in an inactive form back to the synaptic cleft, so that they can return to the axon.

2. The governing equations

Let $c(t,x)$ be the concentration of neurotransmitters, $P(t)$ the fraction of all receptors that are free. Let Ω be the diffusion domain, and Ω_ε be a padding of width ε of the post-terminal membrane where the receptors are considered detached, and $\Omega \cap \Omega_\varepsilon = \varnothing$. Let κ be the diffusion coefficient. This leads to

$$c_t = \kappa \Delta c \quad \text{in } \Omega \tag{1}$$

We assume binding of the neurotransmitter to the receptors can only happen in Ω_ε. Let $r(t,x)$ be the concentration of free receptors in Ω_ε, and let $b(t,x)$ be the concentration of bound receptors. These quantities are connected by the relation

$$\int_{\Omega_\varepsilon} r(t,x) = P(t) \int_{\Omega_\varepsilon} \Big[r(t,x) + b(t,x) \Big] \tag{2}$$

The chemical reaction between receptors and neurotransmitters in Ω_ε is governed by the equation

$$R + N \underset{k_{-1}}{\overset{k_1}{\rightleftharpoons}} B$$

Here N denotes the neurotransmitters, R denotes free receptors, B denotes receptors bound to a neurotransmitter, and k_1 and k_{-1} denotes the reaction rates.
Adding the reaction term to c, together with equations for r and b, we get a system governing the dynamics in Ω_ε as follows.

$$\left.\begin{aligned} c_t &= \kappa \Delta c - k_1 r c + k_{-1} b \\ r_t &= -k_1 r c + k_{-1} b \\ b_t &= +k_1 r c - k_{-1} b \end{aligned}\right\} \text{in } \Omega_\varepsilon \tag{3}$$

3. Characteristic time scale

To get an indication of the time scales of the reactions, the characteristic time scales for

$$c_t^* = \kappa \Delta c^* - k_1 r^* c^* + k_{-1} b^*. \tag{4}$$

is studied. This enables us to get a feeling for the solution of our ODE without having to solve it. The problem is scaled with $c^* = C_0 c, t^* = Tt, x^* = Xx, r^* = Rr$ and $b^* = Bb$.
In one dimension this yield the equation

$$\frac{C_0}{T} c_t = \kappa \frac{c_0}{X^2} c_{xx} - k_1 R C_0 c r + k_{-1} B b. \tag{5}$$

Rearranging the terms gives

$$c_t = \frac{\kappa T}{X^2} c_{xx} - k_1 R T c + k_{-1} B T b. \tag{6}$$

A natural choice for X is the radius of the synaptic cleft, which with the diffusion coefficient κ gives

$$T = \frac{X^2}{\kappa} = 6.05 \times 10^{-8}. \tag{7}$$

Using this T to scale the equations effectively reduces equation (4) to the familiar heat equation $c_t = c_{xx}$.

Now we derive a timescale looking at the two reactions. Having a total number of 193 receptors in a synapse gives a concentration of receptors

$$R = \frac{152}{\pi(0.22 \times 10^{-}6)^2} \frac{1}{m^2} = 9.996 \times 10^{14} \frac{1}{m^2}. \quad (8)$$

Assuming the reaction only takes place in two dimensions, the concentration of free receptors $r(x,t)$ has dimensions $\frac{1}{m^2}$, the reaction coefficient k_1 on dimensionless form is

$$\begin{aligned} k_1 &= 4 \times 10^6 \frac{m^2}{s \cdot mol} \\ &= 4 \times 10^6 \frac{m^2}{6.022 \times 10^{23} s} \\ &= 6.642 \times 10^{-18} \frac{m^2}{s}. \end{aligned}$$

Thus we have

$$T = \frac{1}{k_1 R} = 150.6. \quad (9)$$

This value of T makes the last term of equation (6) dominate and is unphysical.
Now to scaling using the last term. As b is the concentration of bound receptors, a choice for B could be 0.5, the concentration of bound receptors required to trigger transmission. This gives

$$T = \frac{1}{k_{-1} B} = 0.4s. \quad (10)$$

This value of T makes the first term blow up and is also unphysical.

This analysis combined with our knowledge of the nervous system leads us to conclude that $T = 6.05 \times 10^{-8}$ is a feasible time scale for t.

4. Geometrical model assumptions of the synapse

Due to the intercellular space being very thin relative to the terminals, we can reduce the 3D model to a still realistic 2D model. This is illustrated in Figure 1. This reduces computational time drastically. We performed numerical analysis for the 2D case, implying that we are working in Ω_ε.

We first assumed a prism shaped model for the domain for which we are modelling neurotransmitter diffusion and reaction, as this is easily implemented. We reduced the prism to a 2D square, as illustrated in Figure 1.

Upon further examinations, we found that a more reasonable geometrical model for the synapse is a cylindrical shape. This allows us to have circular pre- and post-terminals, which we perceive realistic. We reduced the model to a 2D circle Ω_s where the reaction can happen,

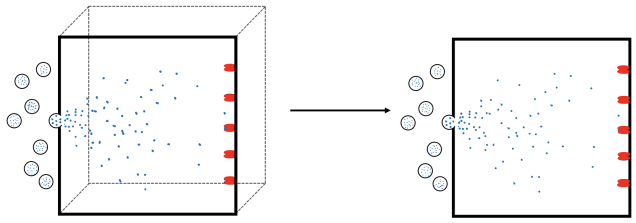

Figure 1: The early 2D model. In this case we assumed a prism, where the width of the prism tended towards zero, leaving us with one square layer of reactions. The model shows the synaptic vesicles releasing neurotransmitters into the synaptic cleft, and the neurotransmitters diffusing in the synaptic cleft and reacting with the receptors.

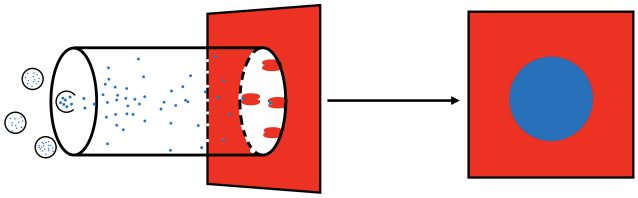

Figure 2: The figure shows the geometrical reduction to Ω_ε in the case of a cylindrical cleft, as used by the numerical implementation. The blue middle section is Ω_s.

with the synaptic cleft being the quadratic domain Ω_ε enclosing Ω_s. The neurotransmitters are free to diffuse inside Ω_ε, however there are only receptors inside Ω_s, thus the reactions can only happen there. This is illustrated in Figure 2.

We first performed numerical analysis using Neumann conditions the boundary $\partial\Omega_\varepsilon$. Thus the neurotransmitters cannot diffuse outside of the synaptic cleft, meaning the flux out of $\partial\Omega_\varepsilon$ is zero. The model was later changed to having Dirichlet boundary conditions, to model the glia cells that are outside of the synaptic cleft. A consequence of this is that the neurotransmitters are free to diffuse out of the synaptic cleft boundary $\partial\Omega_\varepsilon$, but cannot diffuse back into the domain. This is discussed in more technical detail in section 6.

5. Model assumptions

Initially, the neurotransmitters are released through vesicle pops at random locations on the plane Ω_ε. Each vesicle has a radius of about $\rho_v = 20$ nm [3], and the concentration of neurotransmitters inside a vesicle is assumed to be constant. For each model, $C_I = 5000$ neurotransmitters divided evenly across 5 vesicles pops at $t = 0$, and starts diffusing. The initial condition for the concentration $c(0,x)$ can thus be described as

$$c(0,x)\begin{cases}\frac{C_I}{\pi\rho_v^2} & x\in\Omega_{v_i}, i=1,\dots,5\\ 0 & x\in\Omega_\varepsilon\setminus\left(\cup_i\Omega_{v_i}\right)\end{cases},$$

where each $\Omega_{v_i}\subset\Omega_\varepsilon$ denotes a circle of diameter 40 nm randomly positioned in Ω_ε, representing a vesicle pop, and $A_v=\pi\rho_v^2$.

The receptors are initially distributed uniformly on a circle Ω_s of radius $\rho_s=0.22$ μm centered in the middle of Ω_ε. The initial density of free receptors on Ω_s is $R_I=1000$ μm^{-2}. Since this density is distributed uniformly on Ω_s, we can describe the initial concentration $r(0,x)$ as

$$r(0,x)\begin{cases}R_I & x\in\Omega_s\\ 0 & x\in\Omega_\varepsilon\setminus\Omega_s\end{cases}.$$

The initial concentration of bound receptors is set to 0 in all of Ω_ε.

When $P(t)=0.5$, meaning half of the receptors in Ω_ε are bounded, the postsynaptic neuron will be able to forward the signal. Therefore we keep track of this fraction, and estimate that $T_c: P(T_c)=0.5$ is the time it takes for a signal to be transmitted across a synaptic cleft.

6. Numerical schemes for Reaction-Diffusion

Since we have a system of partial differential equations governing concentrations of neurotransmitters and receptors, we found it convenient to use an implicit numerical solver. If we were to choose an explicit method, such as forward Euler, we would be forced to obey stability conditions and to use very small time steps to retain stability. Therefore, an implicit solver is the most feasible option. Observe that the reaction part of the modelling equations introduces non-linearity. Since we rely on linear terms in order to discretize the derivatives in the equation, we need to find a remedy for this. This is tackled by letting the reaction terms be solved explicitly in the numerical solver, that is, calculating it always based on the previous time step.
For general 2D diffusion, we have that

$$\frac{\partial u}{\partial t}=\kappa\left(\frac{\partial^2 u}{\partial x^2}+\frac{\partial^2 u}{\partial y^2}\right). \tag{11}$$

By assuming central difference discretization of the spatial derivatives on the quadratic $n_x\times n_y$ grid as illustrated in figure 3, indexed by $i=1,...,n_x$ and $j=1,...,n_y$, we can write

$$\frac{\partial^2 u}{\partial x^2}\,|_{ij}\approx\frac{u_{i+1,j}-2u_{i,j}+u_{i-1,j}}{\Delta x^2}, \tag{12}$$

$$\frac{\partial^2 u}{\partial y^2}\,|_{ij}\approx\frac{u_{i,j+1}-2u_{i,j}+u_{i,j-1}}{\Delta y^2}, \tag{13}$$

$$\frac{\partial u}{\partial t}\,|_{ij}\approx\frac{u_{ij}^{n+1}-u_{ij}^n}{\Delta t}. \tag{14}$$

u_{1n_y}	...	...	$u_{n_xn_y}$
$\vdots$			$\vdots$
$\vdots$			$\vdots$
u_{11}	...	...	u_{n_x1}

Figure 3: Numerical grid resulting from 2D discretization

By plugging (12)-(14) into (11), we obtain the Crank-Nicholson scheme as

$$\begin{aligned}&(1+4\mu)u_{i,j}^{n+1}-\mu\left(u_{i+1,j}^{n+1}+u_{i-1,j}^{n+1}+u_{i,j+1}^{n+1}+u_{i,j-1}^{n+1}\right)\\&=(1-4\mu)u_{i,j}^n+\mu\left(u_{i+1,j}^n u_{i-1,j}^n+u_{i,j+1}^n+u_{i,j-1}^n\right).\end{aligned} \tag{15}$$

Here we have defined $u_{i,j}^n=u(i\Delta x,j\Delta y,n\Delta t)$ and $\mu=\frac{\kappa\Delta t}{2\Delta x^2}$. μ can be written this way since we are assuming that $\Delta x=\Delta y$.

6.1. Neumann boundary conditions

First, we look at the case in which we enforce concentration conservation on the boundaries of the numerical grid. Let $\vec{n}$ be a unit vector orthogonal to $\partial\Omega_\varepsilon$ at all boundary points. We require that $\nabla c\cdot\vec{n}=0$ at $\partial\Omega_\varepsilon$, such that in the absence of reaction the total amount of neurotransmitters in the domain would be constant at every time step. For concentrations of neurotransmitters c, free receptors r and bounded receptors b, the scheme is as follows

$$\mathbf{A}\mathbf{C}^{n+1}=\mathbf{E}\mathbf{C}^n-\Delta t\mathbf{f}^n \tag{16}$$

$$\mathbf{R}^{n+1}=\mathbf{R}^n-\Delta t\mathbf{f}^n \tag{17}$$

$$\mathbf{B}^{n+1}=\mathbf{B}^n+\Delta t\mathbf{f}^n. \tag{18}$$

Here, $\mathbf{C}^n,\mathbf{R}^n$ and $\mathbf{B}^n$ denotes the concentration of neurotransmitters, bounded and free receptors respectively at time step n. These are $(n_x\cdot n_y)\times 1$-vectors, and takes shape

$$\mathrm{C}^n=\begin{bmatrix}\begin{bmatrix}c_{1n_y}^n\\ \vdots\\ c_{n_xn_y}^n\end{bmatrix}\\ \vdots\\ \begin{bmatrix}c_{12}^n\\ \vdots\\ c_{n_x2}^n\end{bmatrix}\\ \begin{bmatrix}c_{11}^n\\ \vdots\\ c_{n_x1}^n\end{bmatrix}\end{bmatrix}\quad\mathbf{R}^n=\begin{bmatrix}\begin{bmatrix}r_{1n_y}^n\\ \vdots\\ r_{n_xn_y}^n\end{bmatrix}\\ \vdots\\ \begin{bmatrix}r_{12}^n\\ \vdots\\ r_{n_x2}^n\end{bmatrix}\\ \begin{bmatrix}r_{11}^n\\ \vdots\\ r_{n_x1}^n\end{bmatrix}\end{bmatrix}\quad\mathbf{B}^n=\begin{bmatrix}\begin{bmatrix}b_{1n_y}^n\\ \vdots\\ b_{n_xn_y}^n\end{bmatrix}\\ \vdots\\ \begin{bmatrix}b_{12}^n\\ \vdots\\ b_{n_x2}^n\end{bmatrix}\\ \begin{bmatrix}b_{11}^n\\ \vdots\\ b_{n_x1}^n\end{bmatrix}\end{bmatrix}.$$

(19)

$\mathbf{f}^n$ is a vector containing evaluations at each spatial grid-point and at time step n of the function

$$f(c, r, b) = k_1 rc - k_{-1} b. \tag{20}$$

Let $f_{ij}^n = f(c_{ij}^n, r_{ij}^n, b_{ij}^n)$. The vector then takes shape as

$$\mathbf{f}^n = \begin{bmatrix} \begin{bmatrix} f_{1n_y}^n \\ \vdots \\ f_{n_x n_y}^n \end{bmatrix} \\ \vdots \\ \begin{bmatrix} f_{12}^n \\ \vdots \\ f_{n_x 2} \end{bmatrix} \\ \begin{bmatrix} f_{11}^n \\ \vdots \\ f_{n_x 1}^n \end{bmatrix} \end{bmatrix}. \tag{21}$$

The matrix $\mathbf{A}$ has a block structure, and looks like

$$\mathbf{A} = \begin{bmatrix} A_c & A_s & & & \\ A_s & A_d & A_s & & \\ & \ddots & \ddots & \ddots & \\ & & A_s & A_d & A_s \\ & & & A_s & A_c \end{bmatrix}, \tag{22}$$

where

$$A_c = \begin{bmatrix} 1+2\mu & -\mu & & & \\ -\mu & 1+3\mu & -\mu & & \\ & \ddots & \ddots & \ddots & \\ & & -\mu & 1+3\mu & -\mu \\ & & & -\mu & 1+2\mu \end{bmatrix}, \tag{23}$$

$$A_d = \begin{bmatrix} 1+3\mu & -\mu & & & \\ -\mu & 1+4\mu & -\mu & & \\ & \ddots & \ddots & \ddots & \\ & & -\mu & 1+4\mu & -\mu \\ & & & -\mu & 1+3\mu \end{bmatrix}, \tag{24}$$

and

$$A_s = \begin{bmatrix} -\mu & & & & \\ & -\mu & & & \\ & & \ddots & & \\ & & & -\mu & \\ & & & & -\mu \end{bmatrix}. \tag{25}$$

The $\mathbf{E}$ matrix has a similar block structure, with

$$\mathbf{E} = \begin{bmatrix} E_c & E_s & & & \\ E_s & E_d & E_s & & \\ & \ddots & \ddots & \ddots & \\ & & E_s & E_d & E_s \\ & & & E_s & E_c \end{bmatrix}, \tag{26}$$

where

$$E_c = \begin{bmatrix} 1-2\mu & \mu & & & \\ \mu & 1-3\mu & \mu & & \\ & \ddots & \ddots & \ddots & \\ & & \mu & 1-3\mu & \mu \\ & & & \mu & 1-2\mu \end{bmatrix}, \tag{27}$$

$$E_d = \begin{bmatrix} 1-3\mu & \mu & & & \\ \mu & 1-4\mu & \mu & & \\ & \ddots & \ddots & \ddots & \\ & & \mu & 1-4\mu & \mu \\ & & & \mu & 1-3\mu \end{bmatrix}, \tag{28}$$

and

$$E_s = \begin{bmatrix} \mu & & & & \\ & \mu & & & \\ & & \ddots & & \\ & & & \mu & \\ & & & & \mu \end{bmatrix}. \tag{29}$$

Let i^A and j^A denote the i-th row and j-th column of matrix $\mathbf{A}$ respectively. Numerically, to enforce the Neumann boundary conditions, we require that

$$\sum_{j^A=1}^{n_x \cdot n_y} \mathbf{A}_{i^A, j^A} = 1 \quad \forall i^A, \tag{30}$$

and with similar notation for the rows and columns of $\mathbf{E}$, we require

$$\sum_{j^E=1}^{n_x \cdot n_y} \mathbf{E}_{i^E, j^E} = 1 \quad \forall i^E. \tag{31}$$

In a statistical point of view, if we consider the concentration of neurotransmitters to be a probability density function over Ω_ε, the structure of these matrices are chosen such that they works as a normalizing factor ensuring that the concentration still integrates (or sums) to 1 when we propagate in time. With these requirements in place, we now understand why the corner matrices A_c and E_c look like they do.

6.2. Dirichlet boundary conditions

We will now discuss the same numerical scheme as given in (16)-(18), but with Dirichlet boundary conditions. This is closely related to the modelling of glia cells working as a neurotransmitter-cleanser around the synapse. Assuming the same numerical scheme structure, the matrices $\mathbf{A}$ and $\mathbf{E}$ now takes a slightly different form in order to accommodate the Dirichlet conditions. We now have that

$$\mathbf{A} = \begin{bmatrix} I & & & & \\ A_s & A_d & A_s & & \\ & \ddots & \ddots & \ddots & \\ & & A_s & A_d & A_s \\ & & & & I \end{bmatrix}, \tag{32}$$

where I is the $n_x \times n_y$ identity matrix,

$$A_d = \begin{bmatrix} 1 & 0 & 0 & 0 & 0 \\ -\mu & 1+4\mu & -\mu & & \\ & \ddots & \ddots & \ddots & \\ & & -\mu & 1+4\mu & -\mu \\ 0 & 0 & 0 & 0 & 1 \end{bmatrix}, \tag{33}$$

and

$$A_s = \begin{bmatrix} 0 & & & & \\ & -\mu & & & \\ & & \ddots & & \\ & & & -\mu & \\ & & & & 0 \end{bmatrix}. \tag{34}$$

In a similar manner, the $\mathbf{E}$ matrix takes shape

$$\mathbf{E} = \begin{bmatrix} I & & & & \\ E_s & E_d & E_s & & \\ & \ddots & \ddots & \ddots & \\ & & E_s & E_d & E_s \\ & & & & I \end{bmatrix}, \tag{35}$$

with

$$E_d = \begin{bmatrix} 1 & 0 & 0 & 0 & 0 \\ \mu & 1-4\mu & \mu & & \\ & \ddots & \ddots & \ddots & \\ & & \mu & 1-4\mu & \mu \\ 0 & 0 & 0 & 0 & 1 \end{bmatrix}, \tag{36}$$

and

$$E_s = \begin{bmatrix} 0 & & & & \\ & \mu & & & \\ & & \ddots & & \\ & & & \mu & \\ & & & & 0 \end{bmatrix}. \tag{37}$$

With Dirichlet conditions, we are interested in setting the concentration values at $\partial\Omega_\varepsilon$ to a constant value in time. Numerically, this is done by making sure that

$$\mathbf{C}^{n+1}[\text{ind}] = \mathbf{C}^n[\text{ind}] \quad \forall n, \tag{38}$$

where ind is the set of indices that correspond to boundary points in the numerical grid. Since the first and last block vector in $\mathbf{C}$ correspond to the concentrations on the line segments between $(1,1)-(n_x,1)$ and $(1,n_y)-(n_x,n_y)$, an identity matrix in the upper left and lower right corner of the block matrix $\mathbf{A}$ ensures constant concentration values here. Furthermore, by letting every row of $\mathbf{A}$ corresponding to a grid boundary point be an identity row with the 1 placed on the central diagonal, we ensure constant concentration values on the line segments $(1,1)-(1,n_y)$ and $(n_x,1)-(n_x,n_y)$, leading to the modifications done in A_s and A_d.

7. Modelling intercellular fluid flow: Convection-Diffusion-Reaction

The intercellular space between the post and pre-terminal is filled with intercellular fluid. We want to study the effects of an underlying moving fluid on the synaptic transmission. Given that we are working in 2D, denote by $V : \mathbb{R}^+ \times \mathbb{R}^2 \to \mathbb{R}^2$ the vector-valued velocity function which has 3 input arguments: The time t and the spatial position (x, y). For simplicity, we assume that the fluid is moving with constant velocity, so that V is the constant map $v = (v_x, v_y)^T$ on Ω_ε for all t. The modification to the modelling equations is the inclusion of a convection term for modelling intercellular flow.

$$\left.\begin{aligned} c_t &= \kappa\Delta c - V\cdot\nabla c - k_1 rc + k_{-1} b \\ r_t &= -k_1 rc + k_{-1} b \\ b_t &= +k_1 rc - k_{-1} b \end{aligned}\right\} \text{in } \Omega_\varepsilon \tag{39}$$

8. Numerical scheme for Convection-Diffusion-Reaction

Since we now have to incorporate discretized first order derivatives of the concentration of neurotransmitters in the scheme, we get

$$\begin{aligned} \frac{c_{ij}^{n+1} - c_{ij}^n}{\Delta t} = \frac{1}{2}\cdot\frac{\kappa}{\Delta x^2}\left(\delta_x^2 c^{n+1} + \delta_y^2 c^{n+1} + \delta_x^2 c^n + \delta_y^2 c^n\right) - \\ \frac{1}{2}\cdot\frac{1}{2\Delta x}\left(v_x\left[\delta_x c^{n+1} + \delta_x c^n\right] + v_y\left[\delta_y c^{n+1} + \delta_y c^n\right]\right) \end{aligned} \tag{40}$$

where

$$\delta_x^2 c^n = c_{i+1,j}^n - 2c_{i,j}^n + c_{i-1,j}^n \tag{41}$$

$$\delta_y^2 c^n = c_{i,j+1}^n - 2c_{i,j}^n + c_{i,j-1}^n \tag{42}$$

$$\delta_x c^n = c_{i+1,j}^n - c_{i-1,j}^n \tag{43}$$

$$\delta_y c^n = c_{i,j+1}^n - c_{i,j-1}^n, \tag{44}$$

and we again assume that $\Delta y = \Delta x$. The values $v_x = 5$ and $v_y = -5$ are used in the implementation. The scheme can be written in matrix form in the same way as in (16)-(18), where

$$\mathbf{A} = \begin{bmatrix} I & & & & \\ A_l & A_d & A_r & & \\ & \ddots & \ddots & \ddots & \\ & & A_l & A_d & A_r \\ & & & & I \end{bmatrix}, \tag{45}$$

$$A_d = \begin{bmatrix} 1 & 0 & 0 & 0 & 0 \\ -\mu-\sigma_x & 1+4\mu & -\mu+\sigma_x & & \\ & \ddots & \ddots & \ddots & \\ & & -\mu-\sigma_x & 1+4\mu & -\mu+\sigma_x \\ 0 & 0 & 0 & 0 & 1 \end{bmatrix}, \tag{46}$$

$$A_l = \begin{bmatrix} 0 & & & & \\ & -\mu+\sigma_y & & & \\ & & \ddots & & \\ & & & -\mu+\sigma_y & \\ & & & & 0 \end{bmatrix}, \tag{47}$$

and

$$A_r = \begin{bmatrix} 0 & & & & \\ & -\mu-\sigma_y & & & \\ & & \ddots & & \\ & & & -\mu-\sigma_y & \\ & & & & 0 \end{bmatrix}. \tag{48}$$

Similarly, the explicit part of the scheme takes form

$$\mathbf{E} = \begin{bmatrix} I & & & & \\ E_l & E_d & E_r & & \\ & \ddots & \ddots & \ddots & \\ & & E_l & E_d & E_r \\ & & & & I \end{bmatrix}, \tag{49}$$

with

$$E_d = \begin{bmatrix} 1 & 0 & 0 & 0 & 0 \\ \mu+\sigma_x & 1-4\mu & \mu-\sigma_x & & \\ & \ddots & \ddots & \ddots & \\ & & \mu+\sigma_x & 1-4\mu & \mu-\sigma_x \\ 0 & 0 & 0 & 0 & 1 \end{bmatrix}, \tag{50}$$

$$E_l = \begin{bmatrix} 0 & & & & \\ & \mu-\sigma_y & & & \\ & & \ddots & & \\ & & & \mu-\sigma_y & \\ & & & & 0 \end{bmatrix}, \tag{51}$$

and

$$E_r = \begin{bmatrix} 0 & & & & \\ & \mu+\sigma_y & & & \\ & & \ddots & & \\ & & & \mu+\sigma_y & \\ & & & & 0 \end{bmatrix}. \tag{52}$$

Here we have defined

$$\sigma_x = v_x \cdot \frac{\Delta t}{4\Delta x} \tag{53}$$

$$\sigma_y = v_y \cdot \frac{\Delta t}{4\Delta y} \tag{54}$$

while μ is as before.

9. The Laplacian in polar coordinates

Parallel to the work presented in the report, a discretization of the Laplacian operator in polar coordinates was developed and implemented. The idea was to be able to exploit the circular symmetries of the Laplacian in a polar coordinate system, as polar coordinates were also fitting to describe the initial distributions of neurotransmitters and receptors. We eventually decided to stick with a Cartesian coordinate system, but the code for the discretized operator were included in the repository.

Boundary condition	T_c
Neumann	43.8 ns
Dirichlet	44.0 ns
Dirichlet with flow	40.6 ns

Table 1: T_c for different model configurations

10. Results

The results for T_c from the numerical simulations is presented in Table 1.

10.1. Diffusion-Reaction modelling

Plots for the Diffusion-Reaction modelling with Neumann conditions is included in Appendix A. In Plot A.4 the fraction of bounded receptors P is plotted against time. Plots A.5, A.6, and A.7 shows the amount of bounded receptors, free receptors and neurotransmitters respectively, at different times.

Plots for the Diffusion-Reaction modelling with Dirichlet conditions is included in Appendix B. In Plot B.8 the fraction of bounded receptors P is plotted against time. Plots B.9, B.10, and B.11 shows the amount of bounded receptors, free receptors and neurotransmitters respectively, at different times.

10.2. Convection-Diffusion-Reaction modelling

The results of the simulation of the Convection-Diffusion-Reaction equation are provided in appendix C. Plot C.12 shows the fraction of bounded receptors P is plotted against time using Dirichlet boundary conditions. Plots C.13, C.14 and C.15 shows the time development of the amounts of bounded receptors, free receptors and neurotransmitters respectively.

11. Discussion

Comparing our numerical findings with the initial scaling analysis we find that the times until excitation, found in Table 1, has the same order of magnitude as the analytical scaling time.

In the Diffusion-Reaction simulation with Neumann boundary conditions, we observe that the initial distribution of the neurotransmitters are restricted to uniformly distributed vesicle locations. Since we have reduced the geometry to 2D, and thus assuming that the transmitters move immediately to the post-terminal, the transmission

time T_c will only be dependent on the relative difference in location of release point of transmitters and position of receptors on the plane Ω_ε. When time increases, we observe that they diffuse into a more continuous distribution over Ω_ε, which is to be expected. Furthermore, we observe that the peaks in which the transmitters were released at $t = 0$ are somewhat maintained as we progress in time. However, looking at the scales on the z-axis, it is clear that the total amount of free receptors are diminishing and spreads out uniformly across Ω_ε. Looking at the amount of bounded receptors, we see that this is zero initially across Ω_ε as assumed. At later times, the amount of bounded receptors increase most in those areas that contain a high concentration of both neurotransmitter and free receptors. This is to be expected, as more neurotransmitters will react with free receptors compared to areas of lower transmitter-concentrations, leading to a faster growth of bounded receptors in this area. Similarly, the amount of free receptors are decreasing at the same rate as the increase of bounded receptors, and these distributions of receptors can be seen as complementary to each other. We also see the effect of imposing Neumann conditions: The amount of neurotransmitters at $\partial\Omega_\varepsilon$ is not constrained to any value, but the directional derivative of the amounts has to be zero at all boundary points, which is clearly satisfied by looking the Plot A.5, A.6 and A.7.

Using Dirichlet boundary conditions, we see the same behavior in time for transmitters and receptors, but from Figure B.11 we can clearly see the effect of requiring zero amount of transmitters at $\partial\Omega_\varepsilon$. In this case, neurotransmitters are free to flow out of the domain, where they will be collected by glia cells. Thus, the peaks in the neurotransmitter distribution decay faster than in the Neumann case.

When adding flow to the system, the distribution of neurotransmitters behave similarly as in the Dirichlet case, as the same boundary conditions were used. However, we also see a wave forming in the direction of the flow field. In our case, the velocity vector was pointed in such a way that neurotransmitters were transported from their release sites into Ω_s, leading to a faster signal transmission time.

12. Conclusion

Two different geometrical models for the synapse was proposed, and three models for the dynamics were discussed in one of these geometries. The transmission times were estimated for each model. The numerical schemes produced values that reasonably compared to analytically computed time scales of the involved dynamics. Of particular interest was the release of neurotransmitters into the synaptic cleft modelled as discrete vesicle pops, as this lead to a complicated distribution of neurotransmitters in the synapse, even though the modelled domain had a quite simple topology. The introduction of a velocity field to the intercellular fluid also lead to an interesting progression of the neurotransmitter field, moving the distribution peaks across the domain. The work done here could be interesting in for instance the estimation of the probability of synaptic cross-talk, as neurotransmitters could eventually be carried out of the domain and into neighboring synapses.

References

[1] Pascal Wallisch (2014) *Modeling Neurotransmitter Release [online]* Available: `https://www.sciencedirect.com/topics/neuroscience/synaptic-transmission` [Retrieved :09.11.2022]

[2] R.L. Herman (2014) *Numerical Solution of 1D Heat Equation [online]* Available: `http://people.uncw.edu/hermanr/pde1/NumHeatEqn.pdf?fbclid=IwAR3ENCDdQk2le18tD5niJDjzeYfIsP-xKPHxWCM4yXkZbOKV7Mn8DKGlFXk` [Retrived:26.10.2020]

[3] Qu L., Akbergenova Y., et.al. (2009) *Synapse-to-synapse variation in mean synaptic vesicle size and its relationship with synaptic morphology and function* Available: `https://onlinelibrary.wiley.com/doi/full/10.1002/cne.22007` [Retrieved:23.11.2022]

Appendix A. Plots of Reaction-Diffusion simulation with Neumann boundary conditions

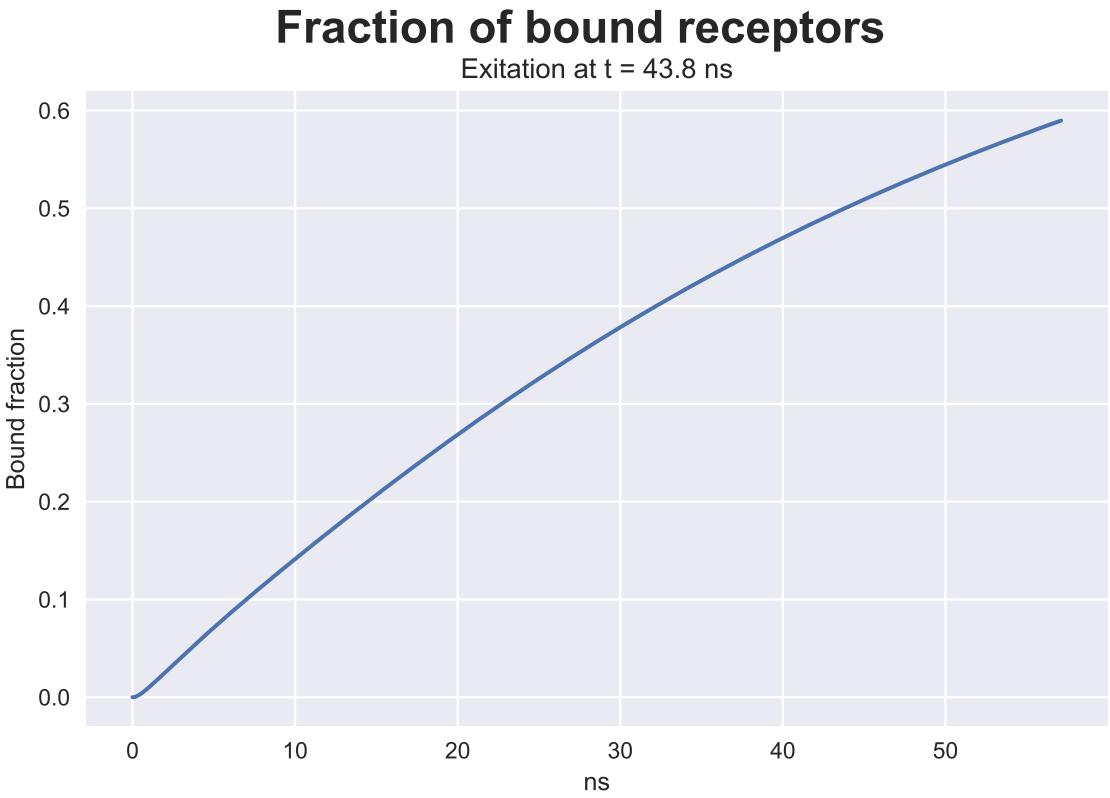

Figure A.4: Fraction P of bound receptors as a function of time t. When $T_c = 43.8$ ns, we have $P = 0.5$ and the signal is released. In this simulation Neumann conditions were used.

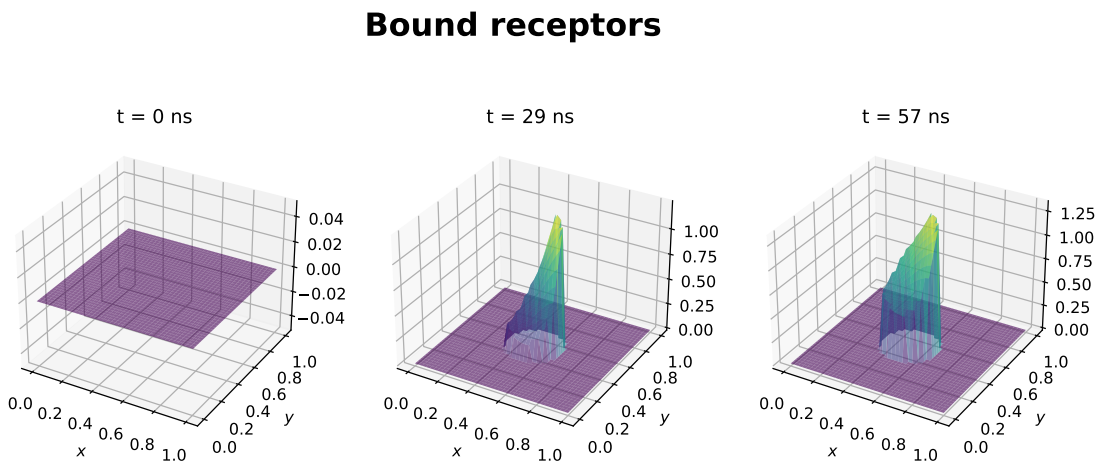

Figure A.5: Amount of bounded receptors on every grid-point in the synaptic cleft, measured at times $t = 0$ ns, $t = 29$ ns and $t = 57$ ns. In this simulation Neumann conditions were used.

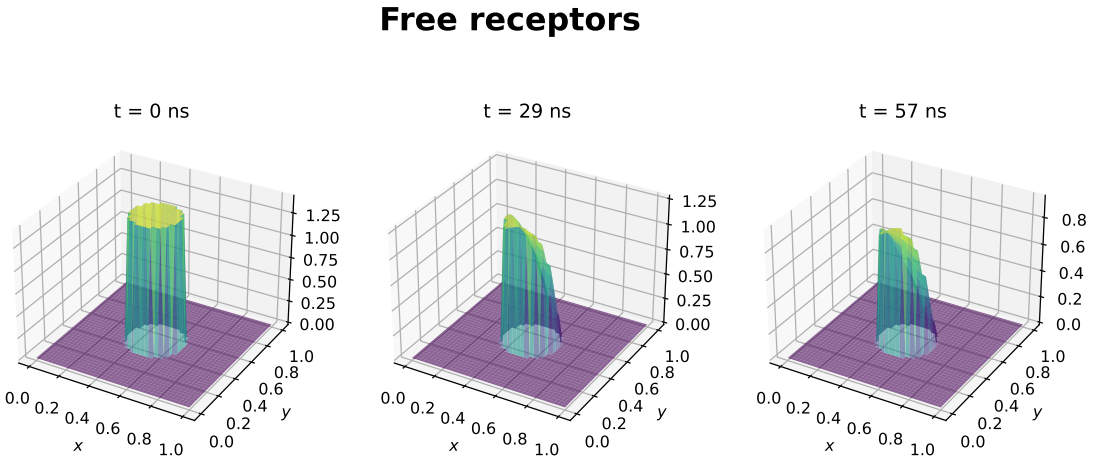

Figure A.6: Amount of free receptors on every grid-point in the synaptic cleft, measured at times $t = 0$ ns, $t = 29$ ns and $t = 57$ ns. In this simulation Neumann conditions were used.

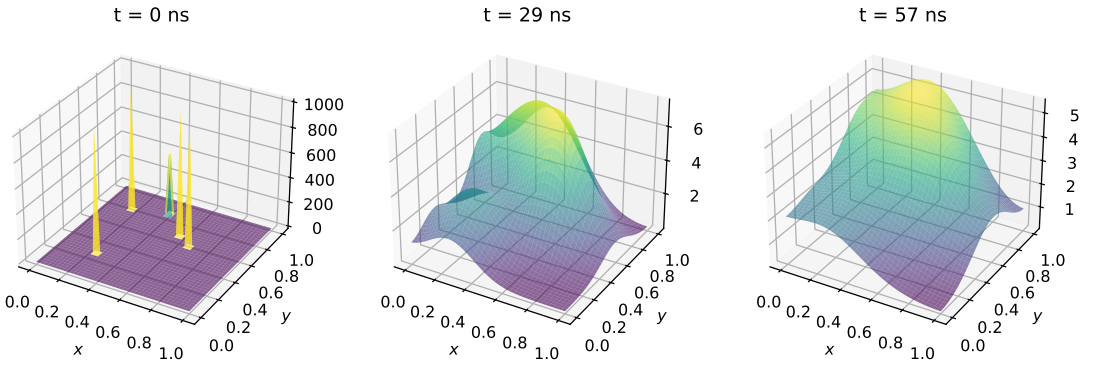

Figure A.7: Amount of neurotransmitters on every grid-point in the synaptic cleft, measured at times $t = 0$ ns, $t = 29$ ns and $t = 57$ ns. In this simulation Neumann conditions were used.

Appendix B. Plots of Diffusion-Reaction simulation with Dirichlet boundary conditions

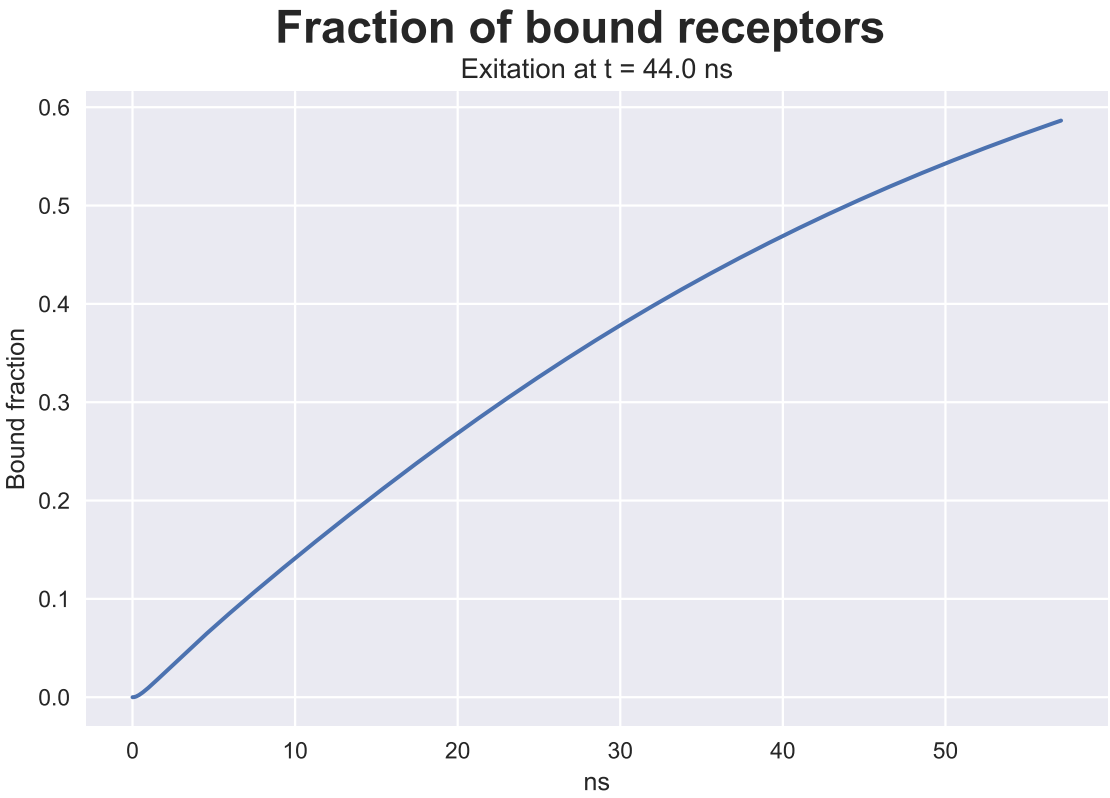

Figure B.8: Fraction P of bound receptors as a function of time t. When $T_c = 44.0$ ns, we have $P = 0.5$ and the signal is released. In this simulatrion Dirichlet conditions were used.

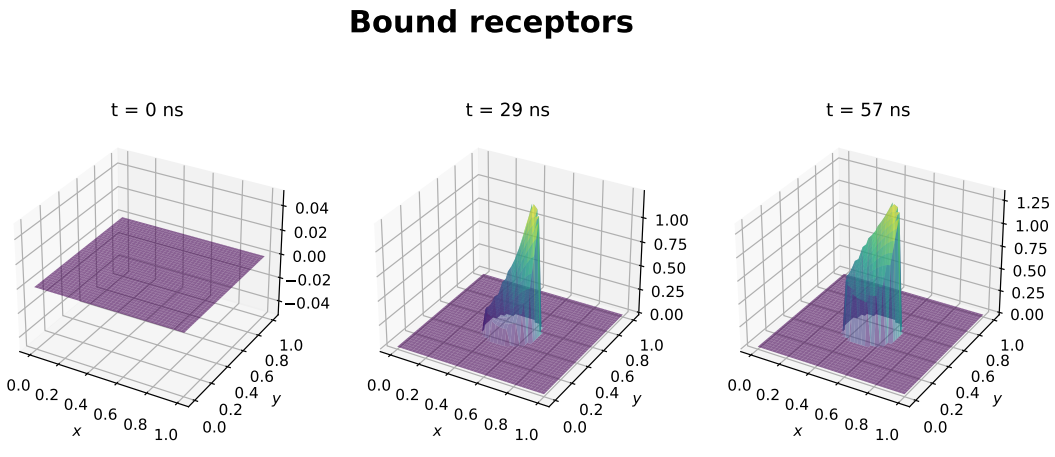

Figure B.9: Amount of bounded receptors on every grid-point in the synaptic cleft, measured at times $t = 0$ ns, $t = 29$ ns and $t = 57$ ns. In this simulation Dirichlet conditions were used.

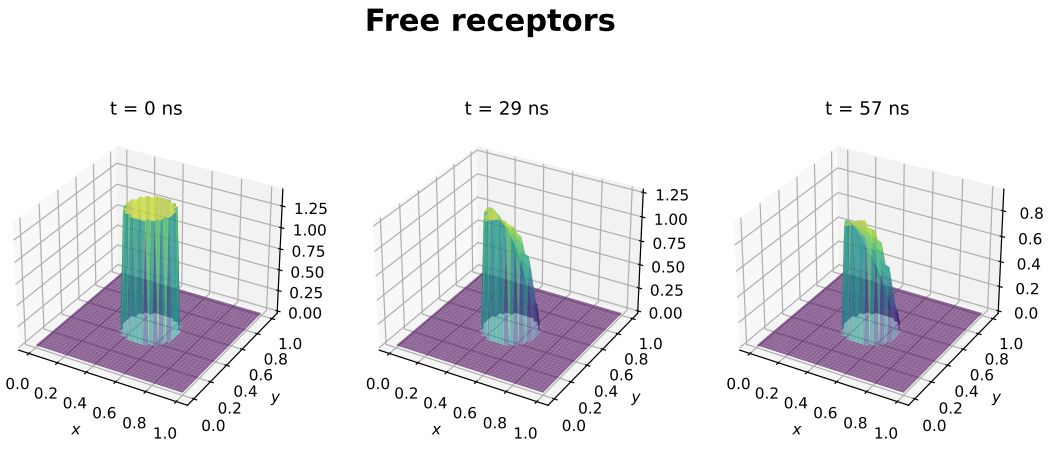

Figure B.10: Amount of free receptors on every grid-point in the synaptic cleft, measured at times $t = 0$ ns, $t = 29$ ns and $t = 57$ ns. In this simulation Dirichlet conditions were used.

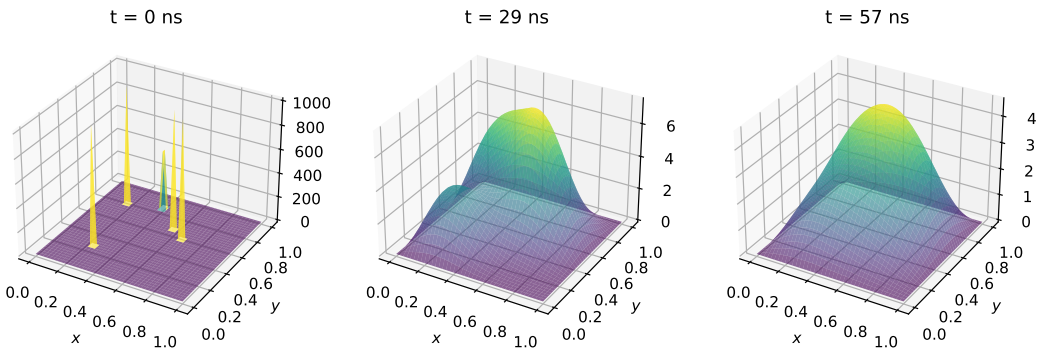

Figure B.11: Amount of neurotransmitters on every grid-point in the synaptic cleft, measured at times $t = 0$ ns, $t = 29$ ns and $t = 57$ ns. In this simulation Dirichlet conditions were used.

Appendix C. Plots of Convection-Diffusion-Reaction simulation with Dirichlet boundary conditions

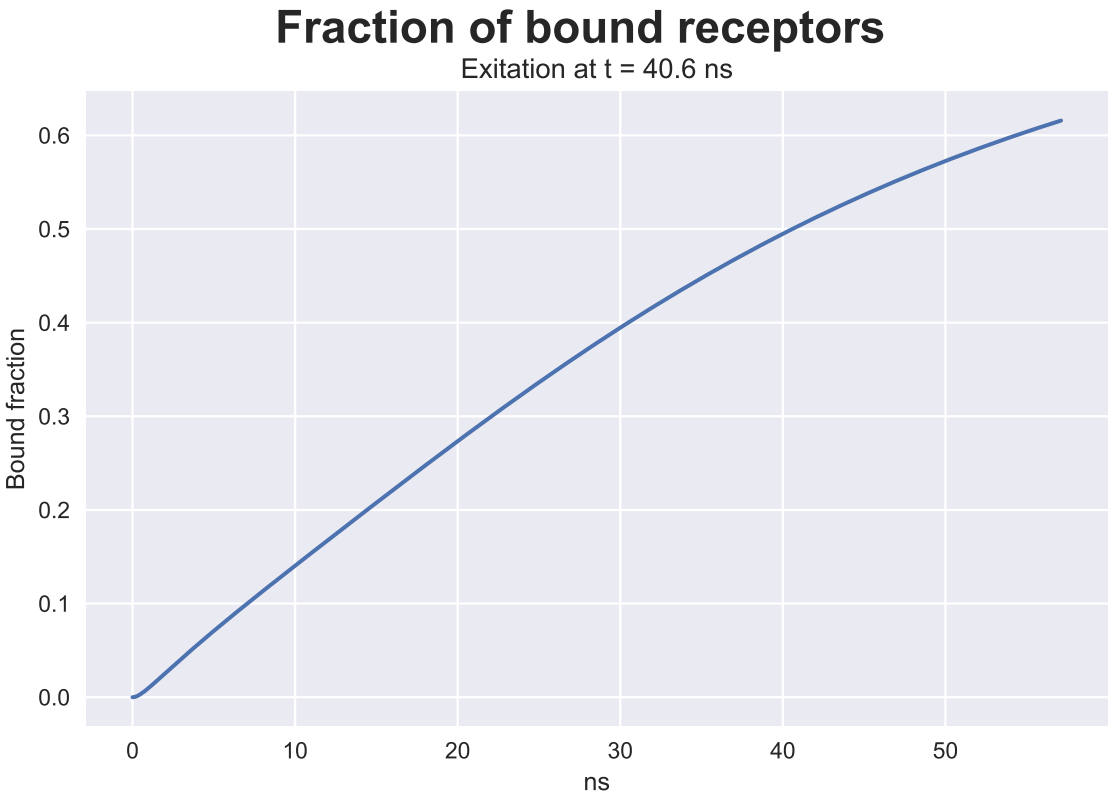

Figure C.12: Fraction P of bound receptors as a function of time t. When $T_c = 40.6$ ns, we have $P = 0.5$ and the signal is released.In this simulation Dirichlet conditions were used with a flow term in the governing equation.

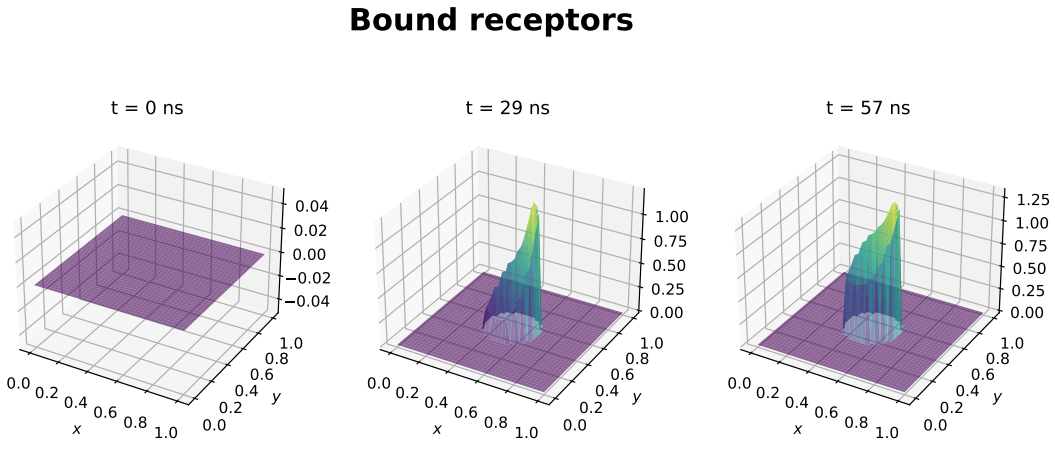

Figure C.13: Amount of bounded receptors on every grid-point in the synaptic cleft, measured at times $t = 0$ ns, $t = 29$ ns and $t = 57$ ns. In this simulation Dirichlet conditions were used with a flow term in the governing equation.

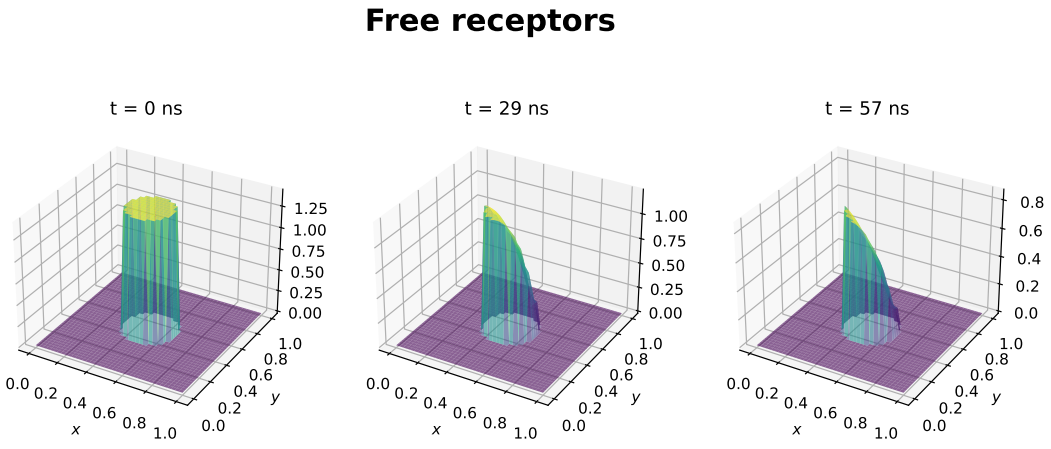

Figure C.14: Amount of free receptors on every grid-point in the synaptic cleft, measured at times $t = 0$ ns, $t = 29$ ns and $t = 57$ ns. In this simulation Dirichlet conditions were used with a flow term in the governing equation.

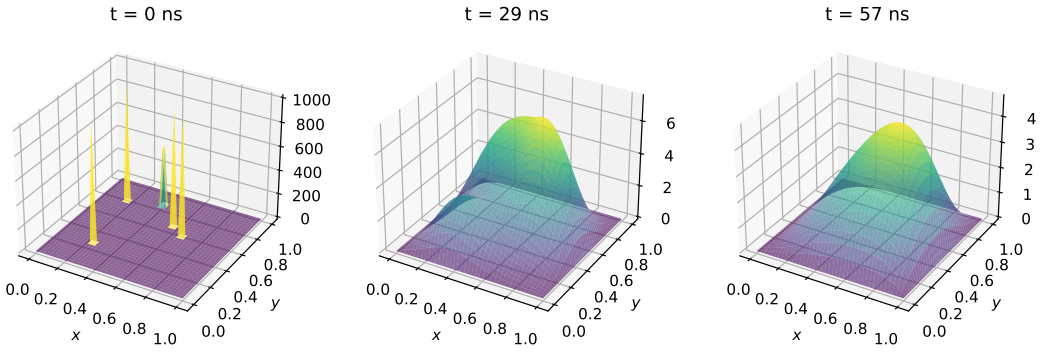

Figure C.15: Amount of neurotransmitters on every grid-point in the synaptic cleft, measured at times $t = 0$ ns, $t = 29$ ns and $t = 57$ ns. In this simulation Dirichlet conditions were used with a flow term in the governing equation.